Supplementary material: Ultra-broadband hyperspectral diffraction imaging using a ptychographic probe

Yikang He[1†], Xianye Li[2,3†], Shuanglong Bian[1], Pengcheng Wang[1], Shixin Hu[1], Shuyan Bi[1], Baoqing Sun[1*]

[1]School of Information Science and Engineering, Shandong University, Qingdao, 266237, China.
[2]School of Mechanical, Electrical and Information Engineering, Shandong University, Weihai, 264209, China.
[3]Shandong Key Laboratory of Intelligent Electronic Packaging Testing and Application, Shandong University, Weihai, 264209, China.

*Corresponding author(s). E-mail(s): baoqing.sun@sdu.edu.cn;
†These authors contributed equally to this work.

Supplementary Note 1: Hyperspectral Reconstruction Results

Figure 1 - 8 show simulation and experiment results for all 34 spectral channels for different objects.

Figure 1 and 2 shows amplitude and phase reconstruction for all 34 spectral channels in the simulation.

Figure 3 shows experimental amplitude reconstruction of the USAF resolution target for all 34 spectral channels.

Figure 4 and 5 shows experimental amplitude and phase reconstruction respectively, of the dendrobium specimen for all 34 spectral channels.

Figure 6 and 7 shows experimental amplitude and phase reconstruction respectively, of the pumpkin specimen for all 34 spectral channels.

Figure 8 shows experimental reconstruction of the spiral phase plate (SPP) for all 34 spectral channels.

Figure 9 shows quantitative analysis of the SPP with mask-amplitude replacement.

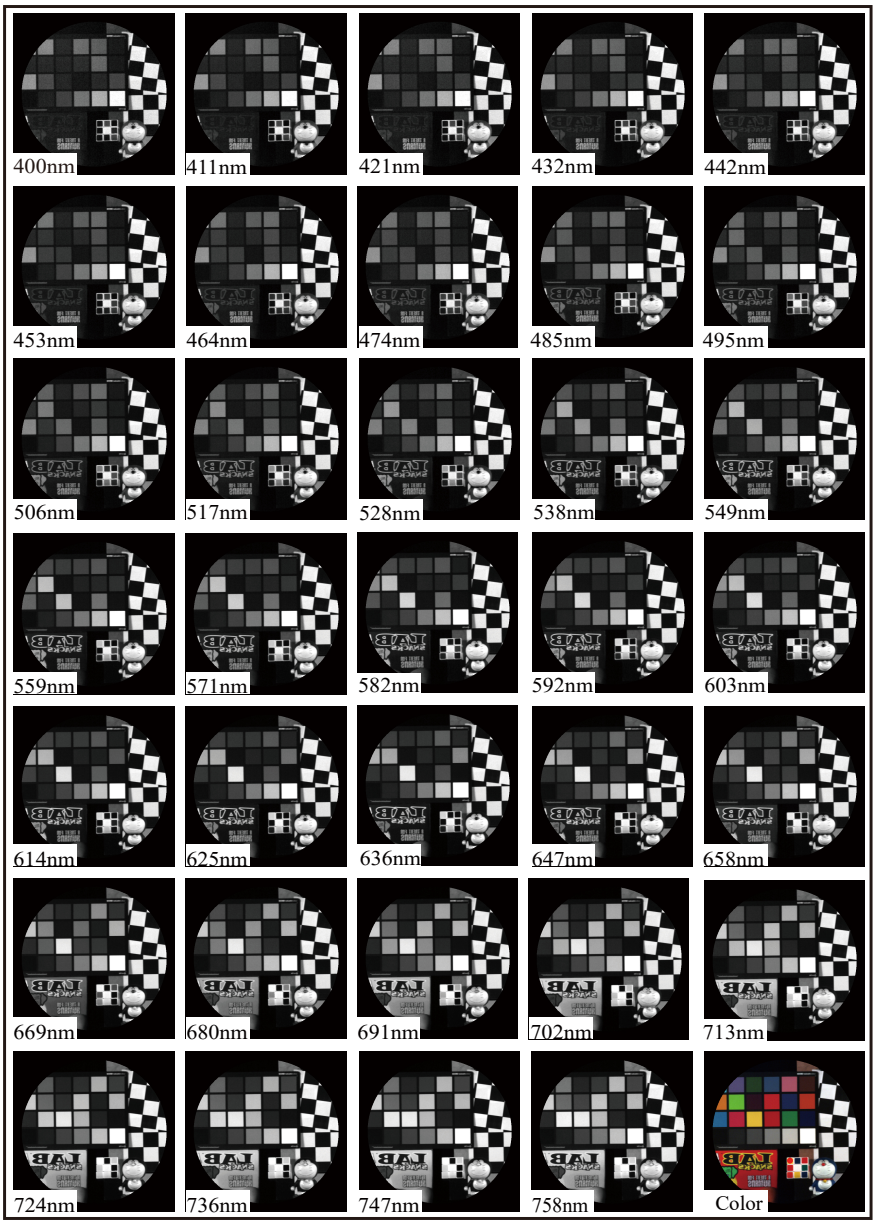

Fig. 1 Simulation amplitude reconstruction of all 34 spectral channels. The bottom right image is the synthesized color image employing all 34 monochromatic ones.

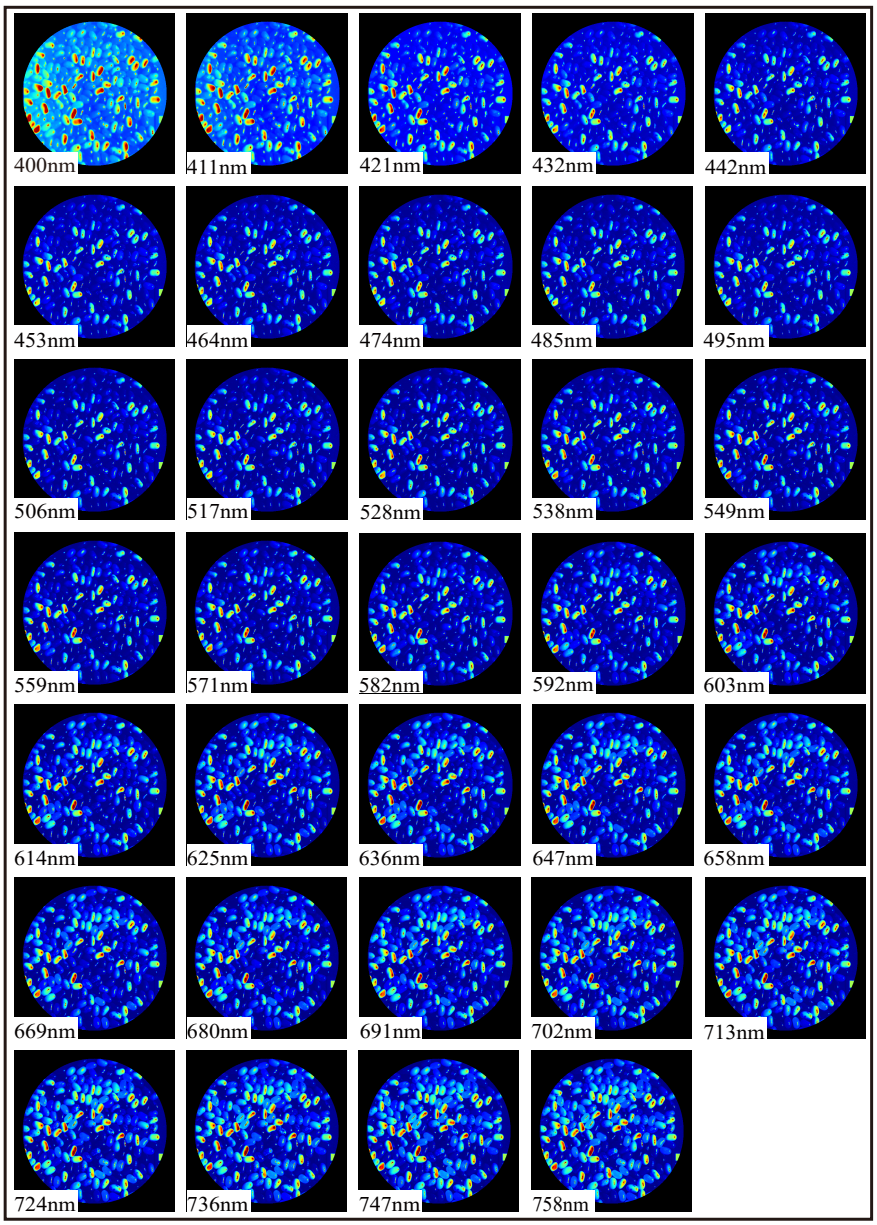

Fig. 2 Simulation phase reconstruction of all 34 spectral channels.

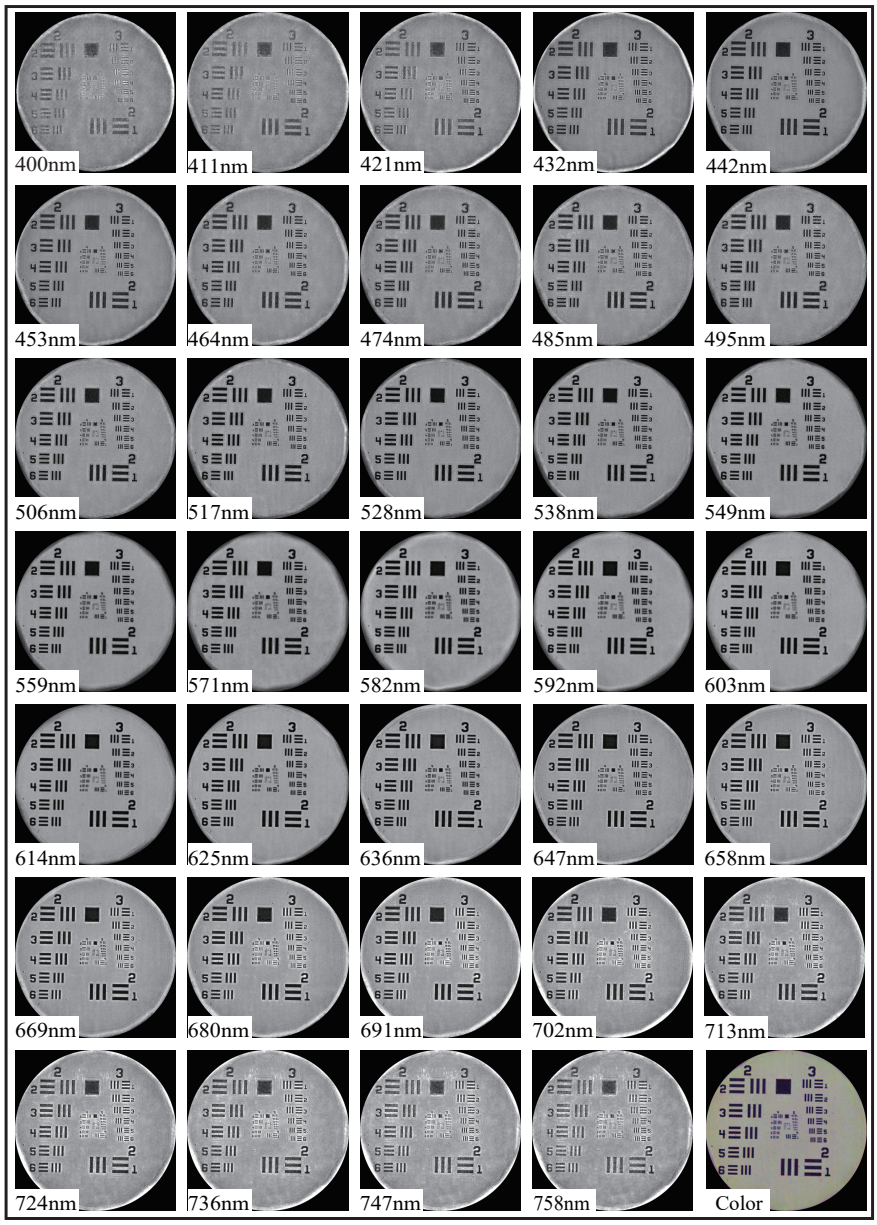

Fig. 3 Experimental amplitude reconstruction of the USAF resolution target for all 34 spectral channels. The bottom right image is the synthesized color image employing all 34 monochromatic ones.

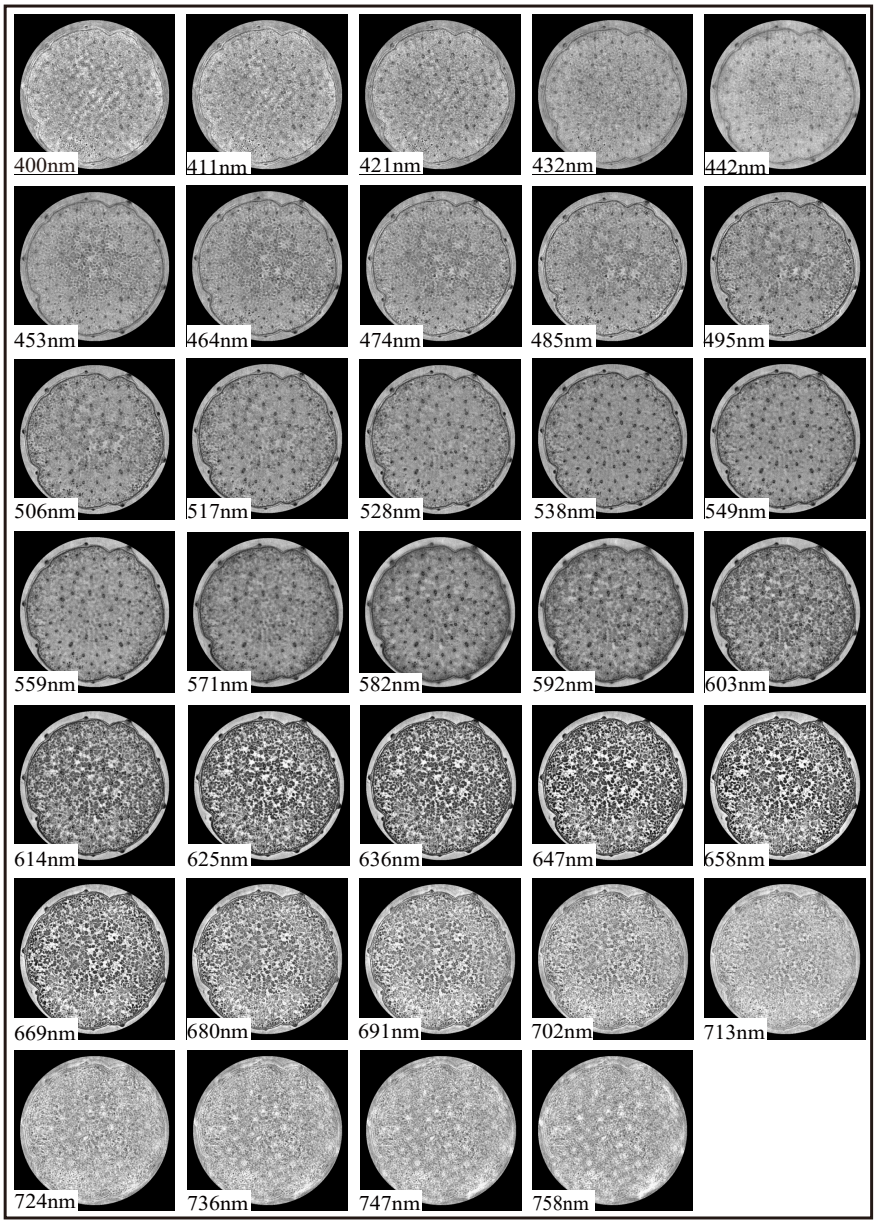

Fig. 4 Experimental amplitude reconstruction of the dendrobium specimen for all 34 spectral channels.

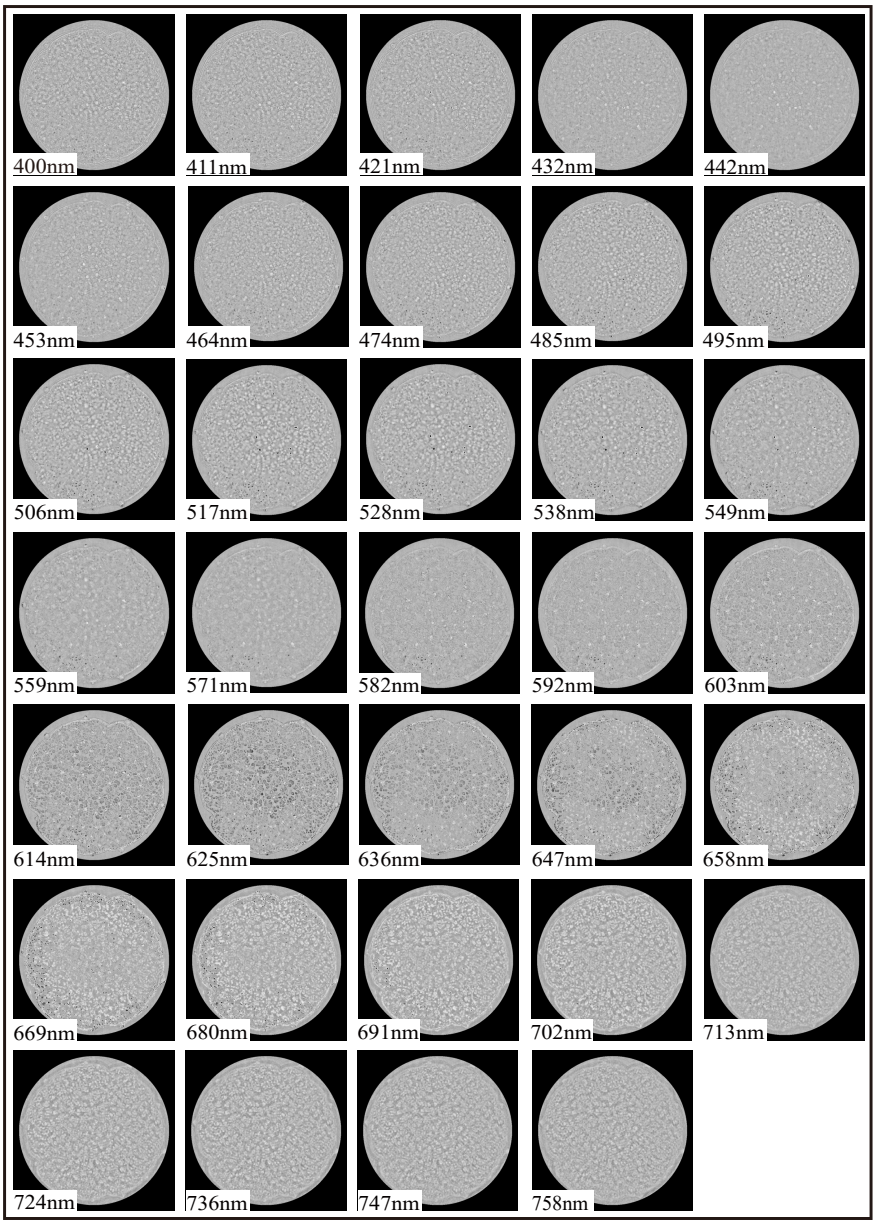

Fig. 5 Experimental phase reconstruction of the dendrobium specimen for all 34 spectral channels.

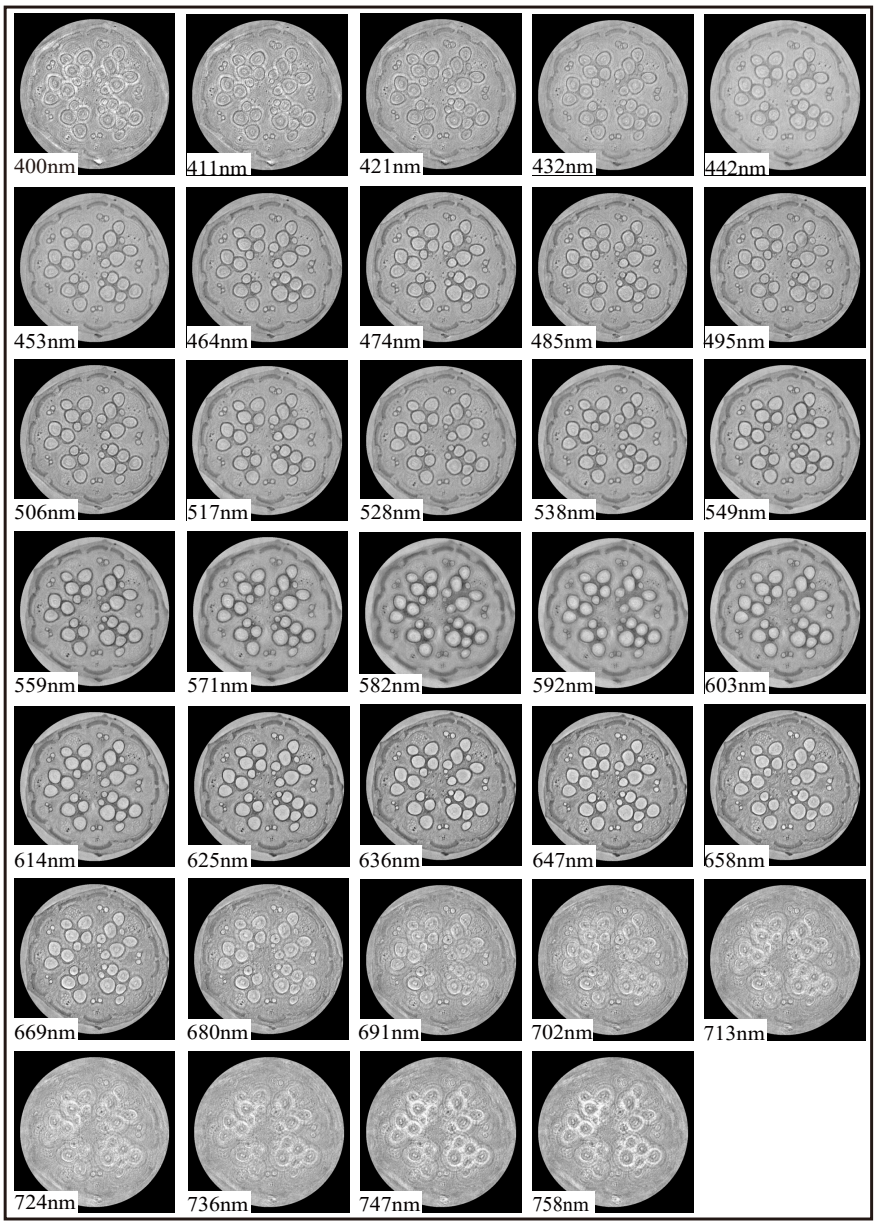

Fig. 6 Experimental amplitude reconstruction of the pumpkin specimen for all 34 spectral channels.

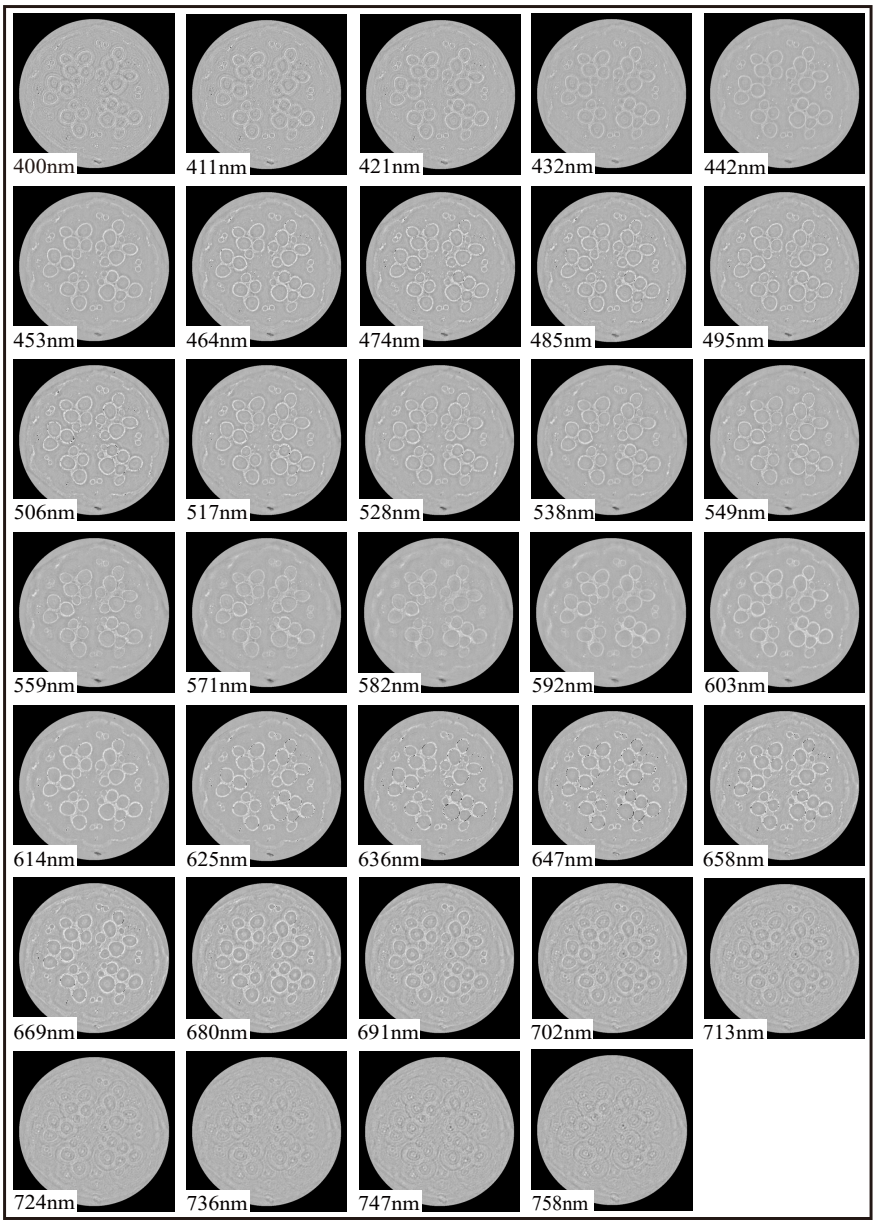

Fig. 7 Experimental phase reconstruction of the pumpkin specimen for all 34 spectral channels.

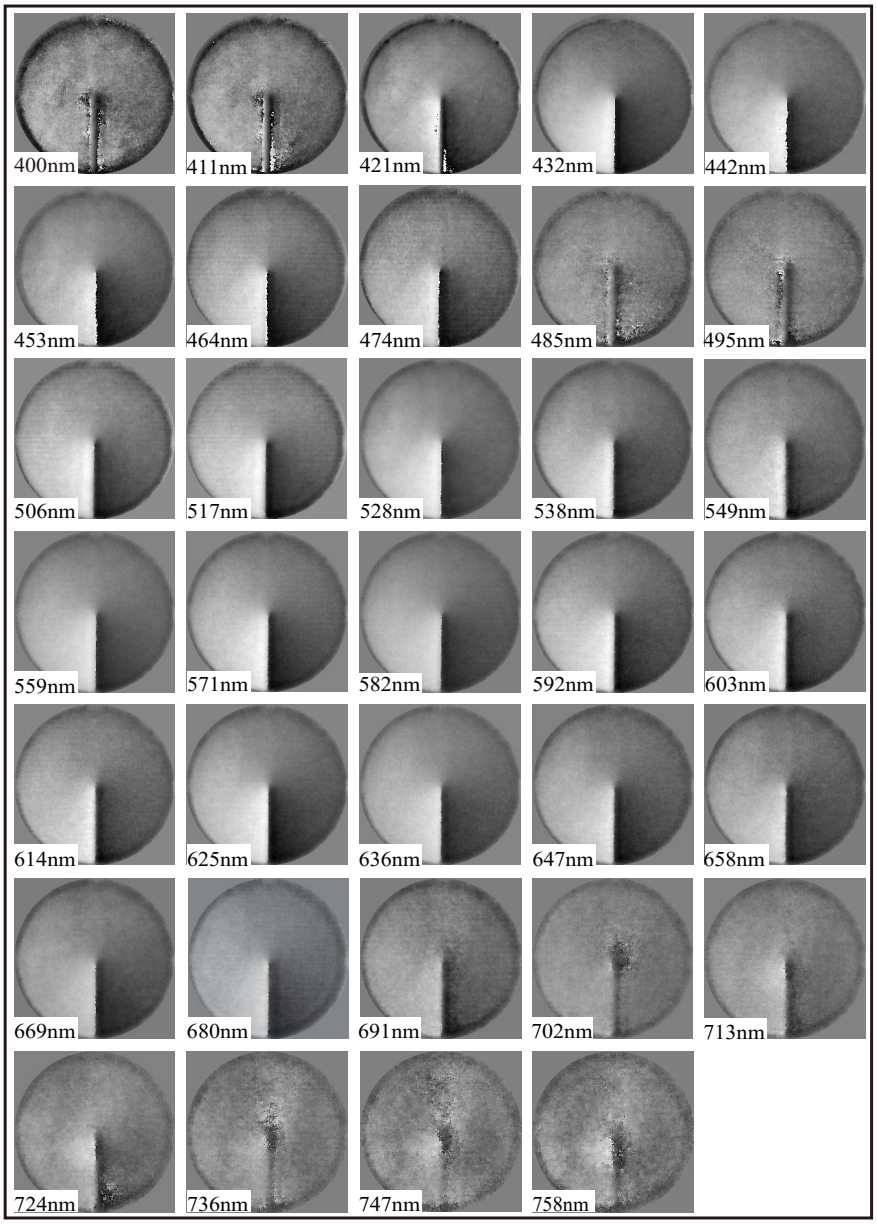

Fig. 8 Experimental phase reconstruction of the SPP for all 34 spectral channels.

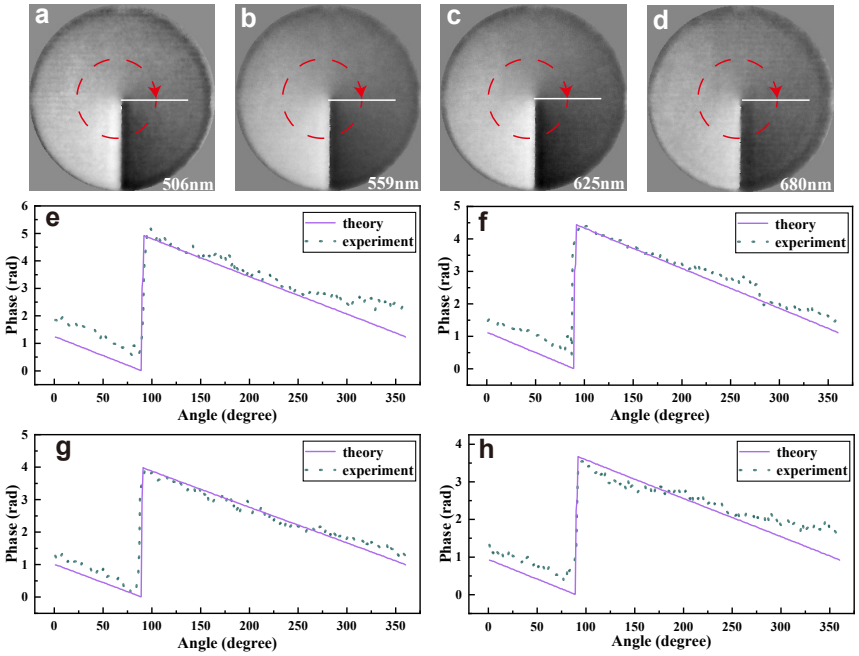

Fig. 9 Reconstruction results and quantitative analysis of the SPP with mask-amplitude replacement. Data is from Fig. 8. (a) - (d) Phase reconstruction images at 506 nm, 559 nm, 625 nm and 680 nm, respectively. (e) - (f) shows the azimuthal results marked with red dash line, compared with ground truth. RMSE of (e)- (h) are 0.3215, 0.2687, 0.2795, 0.3321, respectively.

Supplementary Note 2: Amplitude consistency constraint of the mask

The mask is the important approach to provide extra constrains for the scheme. As stated in the main context, due to the dispersive property of the substrate of the mask, calibration of the mask for all wavelengths becomes nearly impossible. Therefore, we adopt a blind modulation approach. The mask is treated as unknown and gets reconstructed together with the object. An important strategy in the reconstruction is that, we assume a uniform amplitude transmittance across all resolved spectral. In this section we will explain the necessity for uniform transmittance constraint with experimental details.

During the iterative reconstruction process, the mask or object in different spectral channels are reconstructed in parallel without mutual interference. However, due to the uneven input spectral weights and absorption difference from the object, some channels may suffer low signal to noise ratio (SNR) due to insufficient detection energy. Insufficient SNR will ultimately reduce the imaging quality. To address this issue, we take fully advantage of the mask, i.e., the amplitude consistency among all wavelengths, and apply an amplitude consistency constraint over all spectral channels. In

the computational process, we replace the amplitude of the mask at all channels with the one at the peak spectrum, i.e., the wavelength with the highest energy.

To show the benefit for amplitude replacement, we first re-reconstruct the Dendrobium specimen without amplitude replacement using the same data as Fig. 4. The reconstruction results for all 34 spectral channels are shown in Fig.10. Compared to Fig. 5, reconstructions are generally worse with some shadow effect. Especially, images at the last few wavelengths are almost lost.

To further exhibit the influence of spectrum-energy distribution, we conduct reconstruction without amplitude replacement over the SPP data. Results are shown in Fig.11. Corresponding reconstructions of the mask amplitude are shown in Fig. 12. Quantitative analysis at selected wavelengths is shown in Fig.13. Again, reconstructions without mask-amplitude replacement are generally in worse quality. On the other hand, reconstructions of the mask and object exhibit high consistency in quality across the entire spectrum range. In other words, at a given wavelength, if the mask is well-resolved, the object is likely to be imaged with high quality, and vice versa. Because the fused silica has a relative low and constant absorption of light across the whole spectrum, the detected spectrum distribution is similar to that of the illumination input. Therefore, high quality reconstructions always happens at the wavelengths with high illumination energy, a direct demonstration of our assumption that energy level effects the reconstruction quality.

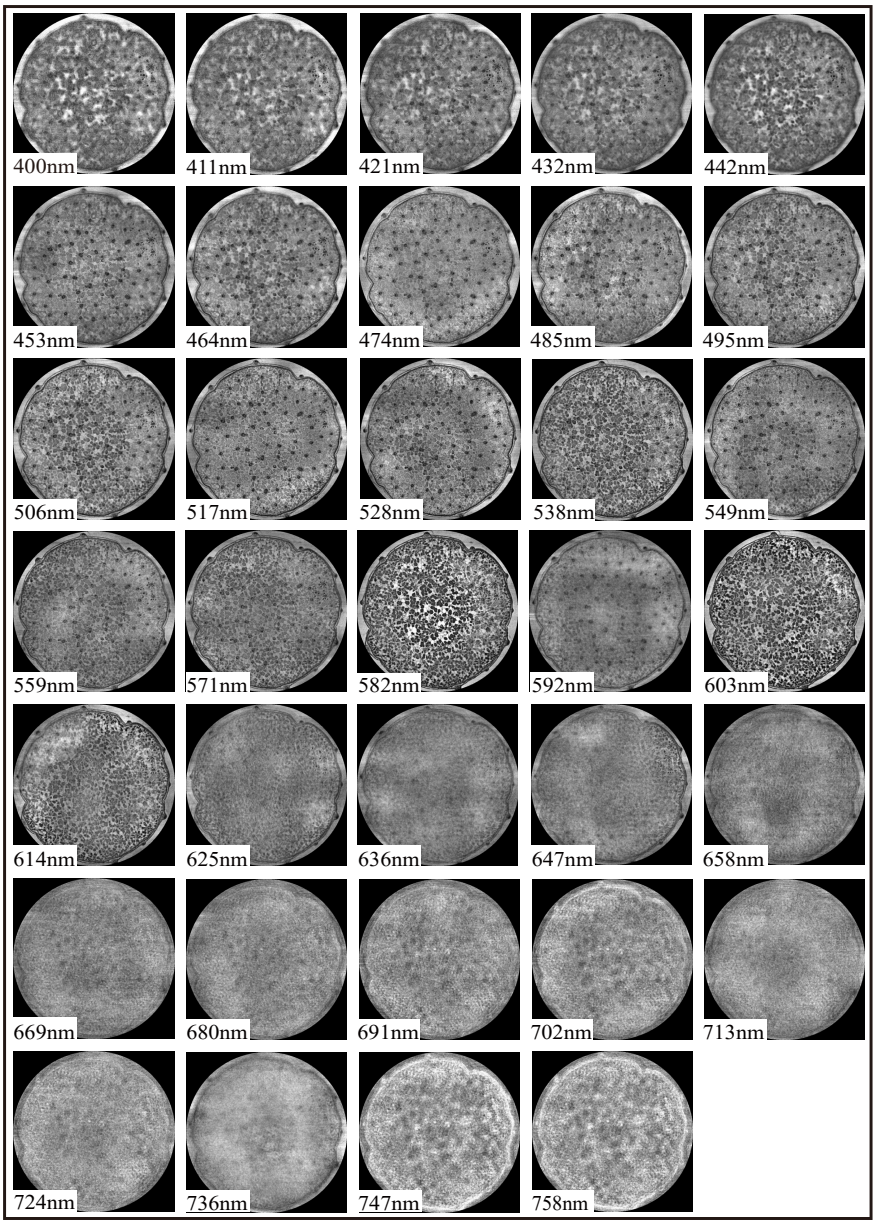

Fig. 10 Amplitude reconstruction results for the 34 spectral bands of the Dendrobium specimen without mask-amplitude replacement.

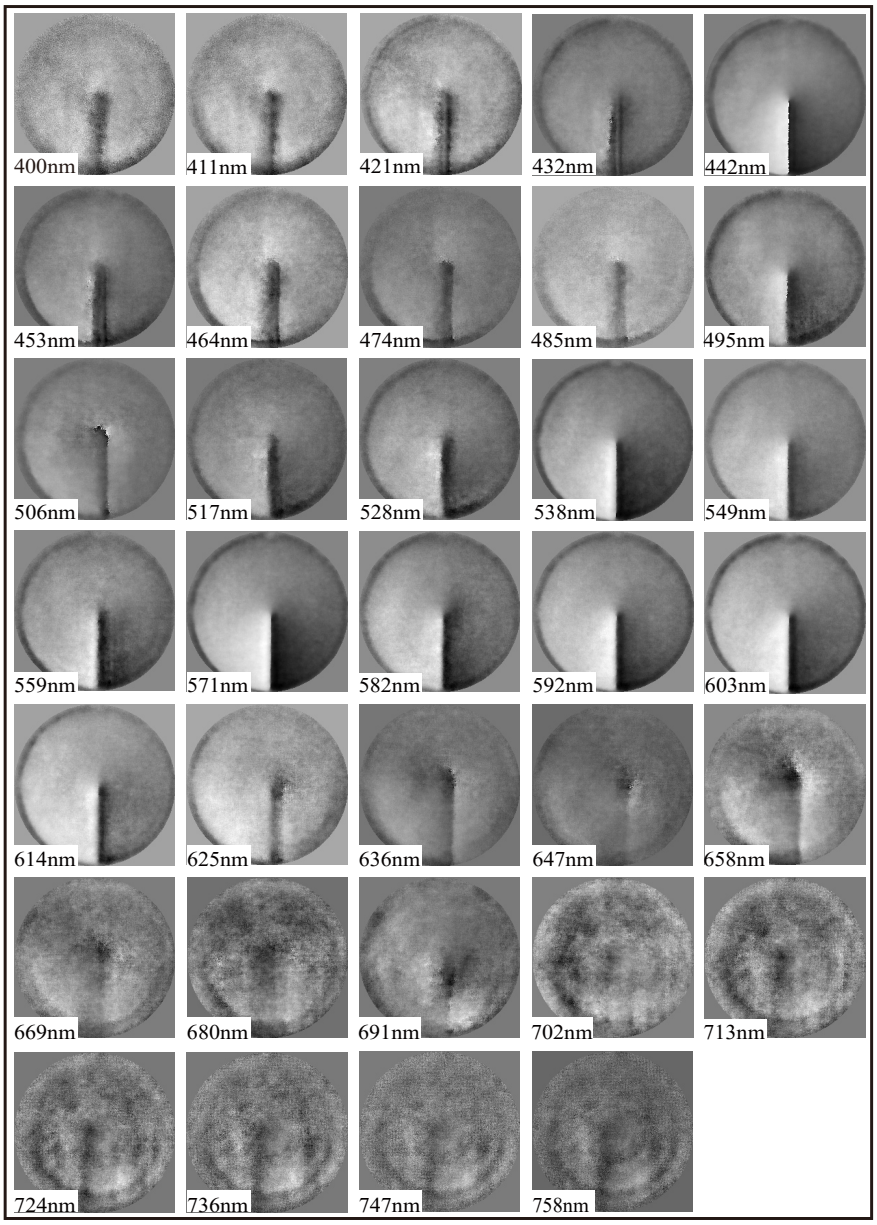

Fig. 11 Phase reconstruction results of the SPP across all 34 spectral bands without mask-amplitude replacement.

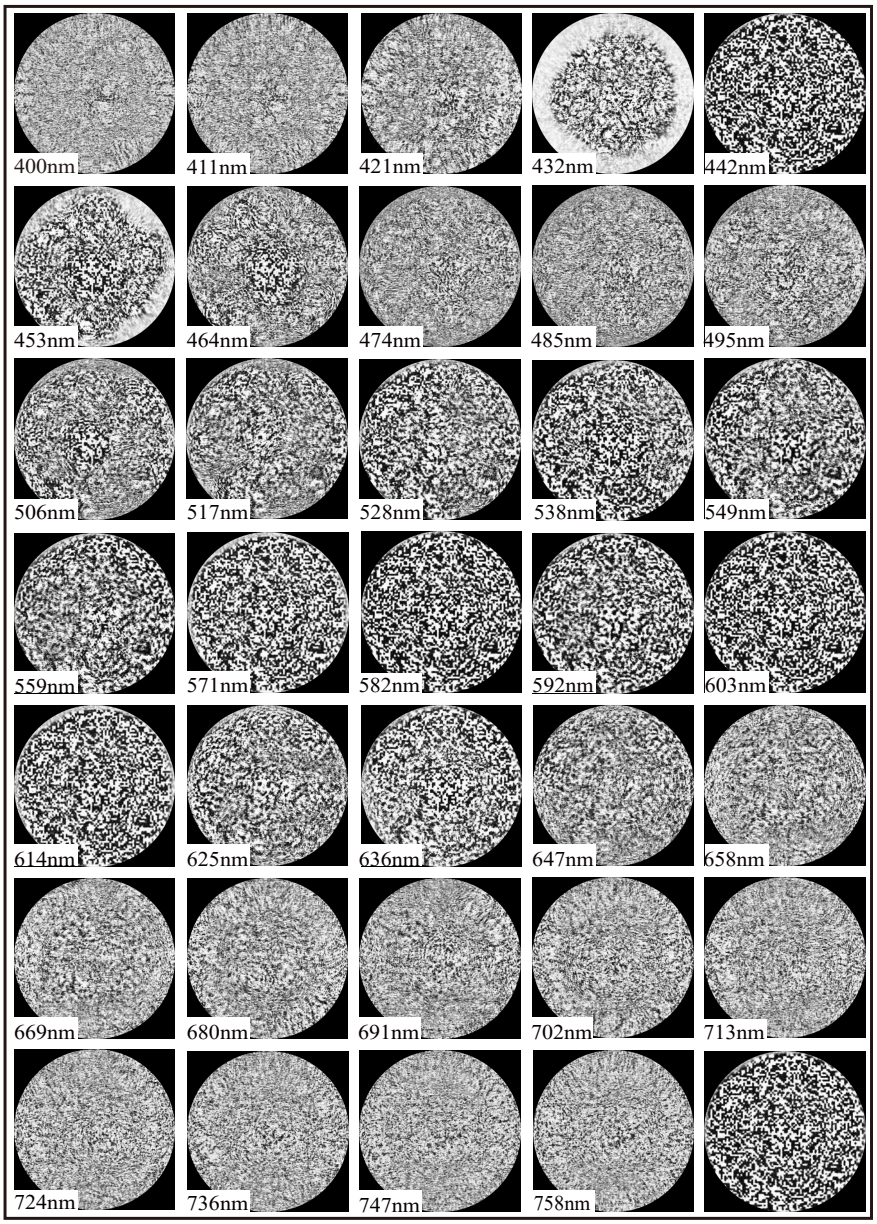

Fig. 12 Amplitude reconstruction results for the 34 spectral bands of the mask without mask-amplitude replacement. The last one on the bottom right is the unique mask in the reconstruction process with mask-amplitude replacement.

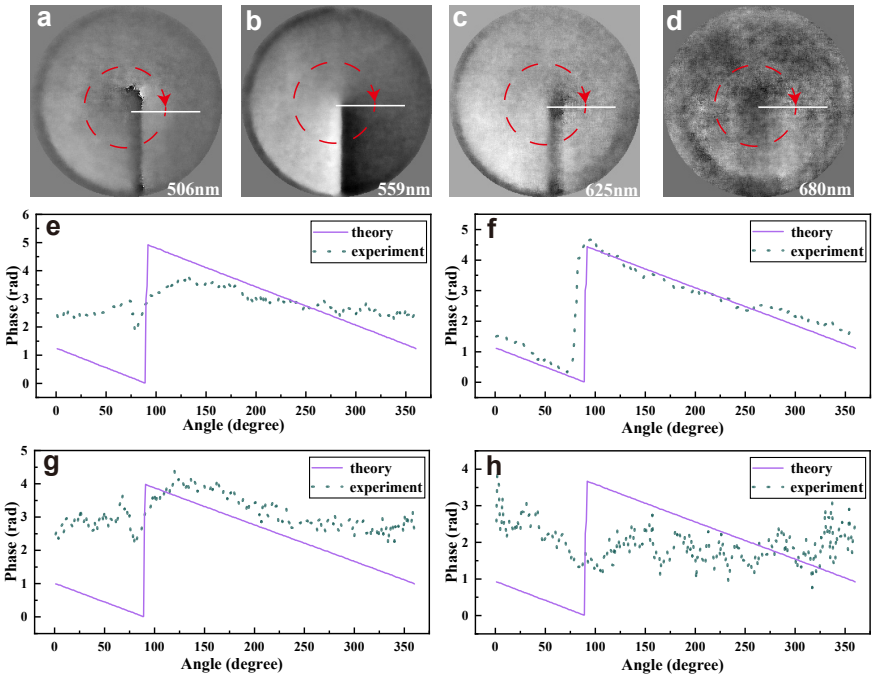

Fig. 13 Reconstruction results and quantitative analysis of the SPP without mask-amplitude replacement. (a) - (d) Phase reconstruction images at 506 nm, 559 nm, 625 nm and 680 nm, respectively. (e) - (f) shows the azimuthal results marked with red dash line, compared with ground truth. RMSE of (e)- (h) are 1.0868, 0.6322, 0.8043, 1.2109, respectively.

Overall, the two comparative experiments demonstrate that the mask amplitude consistency constraint remarkably improves spectral reconstruction quality. We attribute this to the following points. Firstly, replacing the mask amplitude of low-intensity wavelengths with that of the high-intensity band supplies a sharper spatial constraint for the sample at those wavelengths. This addresses a critical limitation: wavelengths with low spectral weight (particularly at spectral extremities) typically yield poorly reconstructed masks, leading to inadequate sample constraints and algorithmic non-convergence. After applying the constraint, even low-weight wavelengths receive a reliable amplitude mask, enabling proper sample reconstruction. Secondly, improved reconstruction of low-intensity spectral components reciprocally enhances high-intensity band reconstruction. This is because the detection constraint provided by the camera as a whole contains information of all spectral channels. Therefore, the estimation of different channels will influence each other. If the reconstruction of low-weight modes increases, their contribution to this coherent sum becomes more physically accurate, thereby strengthening the frequency-domain constraints. This cross-spectral coupling effect ultimately elevates reconstruction accuracy uniformly across all wavelength channels.

Supplementary Note 3: Monochromatic Reconstruction Data

We also conduct a comparison experiment under monochromatic illumination. The experimental setup is the same as the broadband one except that the illumination is replaced by a 633 nm He-Ne laser. Results of different objects are shown in Fig. 14 to 16.

Fig.14 presents the reconstruction results of a USAF resolution target under monochromatic light illumination. Fig.14(a) shows the reconstructed illumination beam profile, while Fig.14(b) displays the reconstructed resolution target with an enlarged view (red dashed box) highlighting the fifth group of resolution elements. The phase profile of the target is shown in Fig.14(c). Figure 14(d) shows the reconstructed mask pattern. For quantitative evaluation, Fig. 14(e) plots the intensity distribution across the resolution elements marked by the dashed line in the enlarged area of Fig.14(b), demonstrating an imaging resolution of 8.77 μm. These results confirm robust amplitude and phase fidelity of our reconstruction.

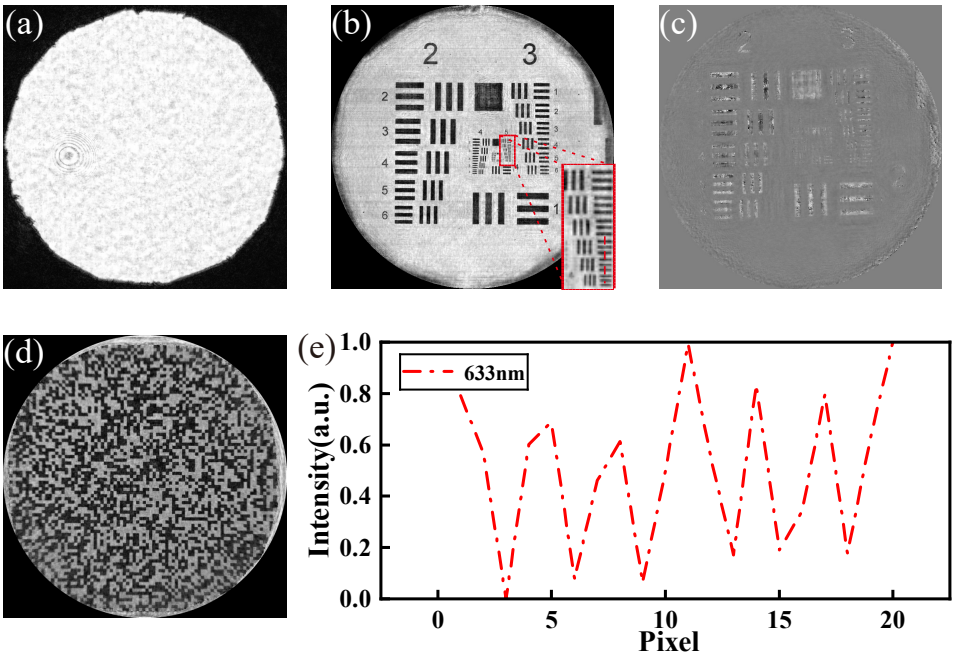

Fig. 14 Reconstructions of USAF resolution target under monochromatic light illumination. (a) Reconstructed illumination beam. (b) Reconstructed resolution target, with the lower right corner (enclosed in red dashed lines) showing an enlarged view of the fifth group of elements. (c) Phase reconstruction of the resolution target. (d) Reconstructed mask. (e) Reconstruction values of the elements marked by the red dashed line in the enlarged area in Figure (b), indicating an imaging resolution of 8.77 μm.

Figure 15 displays the reconstruction results of the SPP under monochromatic illumination. The ground truth is shown in Fig.15(a). Figure 15(b) and (c) display the reconstructed amplitude and phase distributions, respectively. Figure 15(d) provides a three-dimensional visualization of the reconstructed SPP, highlighting its helical wavefront structure. Quantitative validation is shown in Fig.15(e), where phase values along the red dashed line in (c) are plotted. RMSE is calculated as 0.1733 in respect to the ground truth, demonstrating a high reconstruction precision of the scheme.

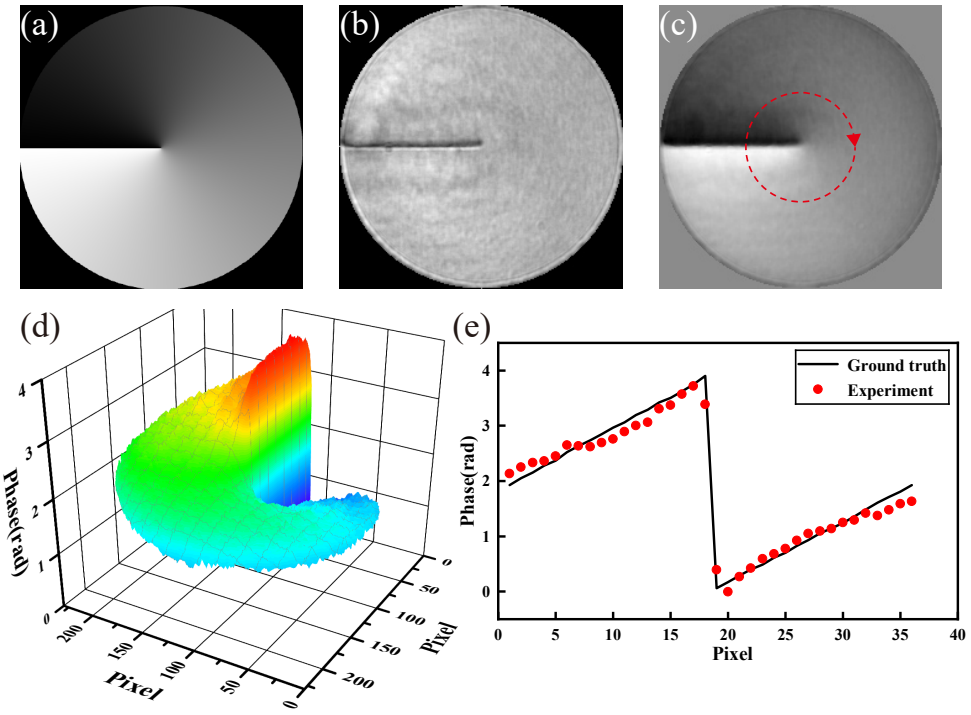

Fig. 15 Reconstructions of SPP under monochromatic light illumination. (a) Ground truth; (b) Reconstructed amplitude; (c) Reconstructed phase;(d) Three-dimensional visualization of the reconstructed SPP; (e) Phase values along the red dashed line in (c), where red dots indicate the reconstructed phase values and the black line indicates the theoretical values, and the RMSE is 0.1733.

Figure 16 shows the reconstruction results of two biological specimen under monochromatic illumination.

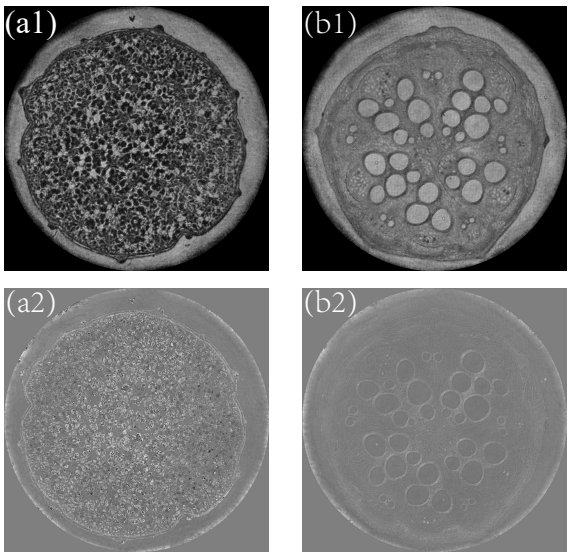

Fig. 16 Reconstructions of biological samples under monochromatic light illumination. (a1) Amplitude reconstruction of Dendrobium specimen cross-section; (a2) Phase reconstruction of Dendrobium specimen cross-section; (b1) Reconstructed amplitude of pumpkin stem cross-section; (b2) Reconstructed phase of pumpkin stem cross-section;